Chapter 1: Overview

1.0 Introduction

This thesis concerns observation of magnetic resonance phenomena through measurements of magnetically induced mechanical oscillations. The principal result of this work is a new class of detectors and methods that promises to extend the applicability of nuclear magnetic resonance (NMR) for chemical analysis and imaging to samples and problems that are currently inaccessible by NMR due to the poor sensitivity of traditional methods at reduced size scales.

NMR is known by its practitioners as a method of finely detailed non-destructive chemical analysis or as a tool for non-invasive medical imaging. But at the most fundamental level, nuclear magnetic resonance is the resonant reorientation of nuclear moments by applied magnetic fields. The reorientation of nuclear moments in a sample produces changes in the sample's magnetization as a function of applied electromagnetic stimuli, such stimuli most often taking the form of pulses of radio-frequency (rf) fields. The dynamics of the sample's spin system are registered by a detection apparatus as changes in the weak magnetic field produced by the sample. Leaving aside the so-called "trigger methods" of magnetic resonance[1], and optical methods that are peculiar only to a very narrow range of

samples or conditions[2-4], NMR devices are therefore essentially *magnetometers* connected to ancillary apparatus of varying degrees of sophistication.

Three types of detection schemes are commonly used to measure the magnetization of a sample (or its susceptibility). The first type of detector, an induction coil, forms the basis of all commercial NMR spectrometers and magnetic resonance imagers. Coherent precession of a sample's magnetization produces a change in the magnetic flux linking a nearby or enclosing coil. The resulting electromotive force in the coil, produced in accordance with Faraday's law, is amplified and analyzed.

A second type of detector is the superconducting quantum interference device (SQUID). The static magnetic flux through a superconducting loop disposed near the sample causes a change in the relative phase of two parts of an electron's wavefunction as those parts coherently traverse two separate paths around the loop. Recombination of the two parts of the wavefunction can occur in phase or out of phase, and as a result, the conductance of the device depends upon the flux linking the loop, and therefore on the magnetization of the sample. This physics forms the basis of SQUID magnetometers, which are used for static or low-frequency magnetometry[5,6]. SQUIDs have also been used in low-field NMR and nuclear quadrupole resonance (NQR)[7,8].

A third type of detector is the *force detector.* Any magnetized body that either moves in response to magnetic forces exerted by the sample or that forces the sample itself to move falls into this class. Force detection is the oldest method

of magnetometry/susceptometry. It is the basis for the Gouy balance[9,10] and for the vibrating-sample magnetometer[11]. It was also the basis for the very first method of magnetic *resonance spectroscopy* in the form of Rabi's molecular beam method[12]. Despite this long history, here we take a fresh look at detection of magnetic resonance with mechanical means.

1.1 Better Observation of Magnetization, Enhanced Resolution, and No Gradient (BOOMERANG)

Figure 1.1 shows a spherical sample enclosed inside an idealized flexible magnetic "detector" in the shape of a hollowed-out sphere. The magnetizations of the sample and the detector are aligned along the same axis. The sample exerts magnetic forces that tend to distort the detector as those dipole elements in the detector near the "poles" of the sample are attracted axially, while those near the "equator" are repelled laterally. Cyclic inversion of the sample's magnetization (discussed in Chapter 3) reverses the sign of the forces, alternately compressing and extending the flexible detector along its magnetization axis.

This mechanical detector is ideal in the sense that at no time is there a field gradient inside the sample volume, no matter how large the elliptical distortion of the spherical detector along its magnetization axis.

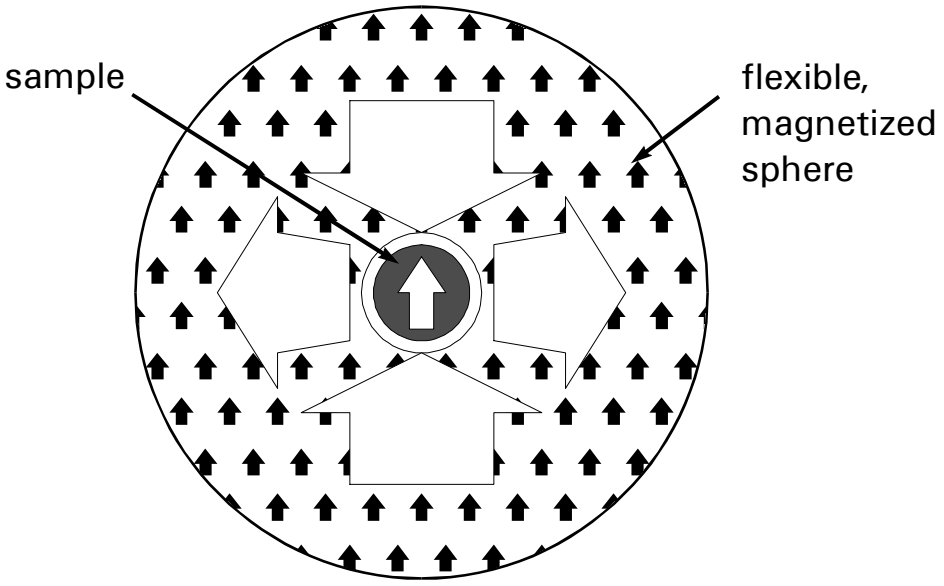

Figure 1.1. Flexible-sphere model of idealized mechanical detector. The sample is surrounded by a hollowed sphere of flexible magnetic material, and both are magnetized as shown by the vertical arrows. The sample exerts forces on individual dipole elements in the detector material, and these forces distort the detector along its symmetry axis.

Figure 1.2 shows a single cylindrical magnet above a spherical sample. Both the magnet and the sample are magnetized along the symmetry axis of the cylinder. The magnet is bound to a flexible suspension that provides for it a high-quality harmonic motion along its symmetry axis. Cyclic inversion of the sample's magnetization may be used to modulate the force coupling the sample and the magnet, resonantly driving this harmonic oscillation. The arrangement of sample, magnet, and suspension is reproduced inside an assembly of other

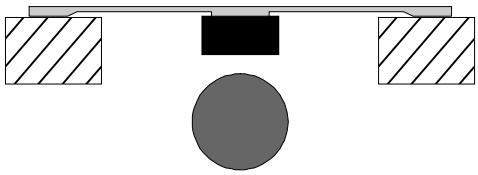

Figure 1.2. Cylindrical detector magnet bound to an anchored, flexible suspension and disposed near a spherical sample.

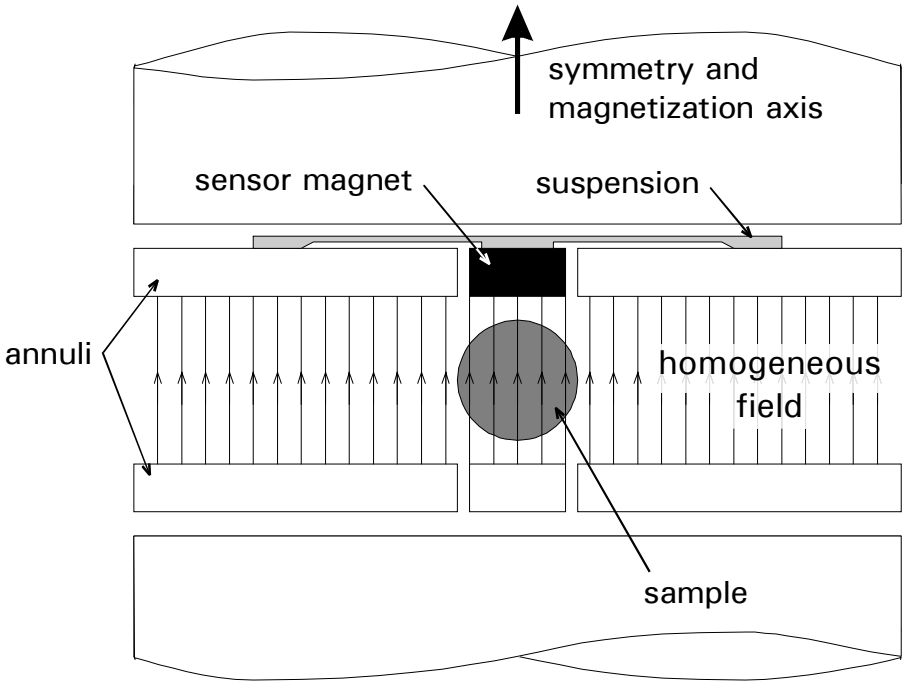

Figure 1.3. Magnet assembly incorporating the sensor magnet and flexible suspension of Figure 1.2. All the magnets in the assembly are magnetized along the common axis of cylindrical symmetry, which is vertical in the figure. The dimensions of the magnets are chosen so that the magnetic field throughout the sample volume is as homogeneous as possible, such homogeneity being limited by the smallest possible spacing between the sensor magnet and surrounding annulus. Reflection symmetry across the horizontal plane through the sample nulls odd-order field gradients.

magnets, all polarized along the common axis of cylindrical symmetry, in Figure 1.3, with the single magnet of Figure 1.2 now designated as a "sensor magnet."

In this geometry, the axial oscillation of the sensor magnet takes place inside an annular magnet, with the height of these two magnets the same, their faces flush when the sensor magnet is at the equilibrium point of its axial motion. The totality of the magnets in the assembly provides for the sample a homogeneous field that, by design, approximates the homogeneity of the idealized spherical case of Figure 1.1.

In both the idealized geometry of Figure 1.1 and in the cylindrical geometry of Figure 1.3, the latter being motivated by the practical concerns of ease of fabrication and sample access, we have emphasized the homogeneity of the magnetic field throughout the sample volume. The experimentally observed fact that the sensor magnet of Figure 1.3 can be made to oscillate in response to modulation of the sample's magnetization shows that the ability to measure susceptibility and magnetic resonance with force detection *is entirely independent of any field gradient in the sample volume.* This view, which is in contrast to the conceptual development of other force-detection methods (briefly surveyed in Appendix A), is the central theme behind the method of magnetic resonance now called Better Observation of Magnetization, Enhanced Resolution, and No Gradient (BOOMERANG)[13,14].

1.2 Problems Caused by Field Inhomogeneity

The BOOMERANG method solves several problems associated with large gradients in the sample volume. Without the annular and other magnets of Figure 1.3, the sensor magnet's own inhomogeneous field spreads the Larmor frequencies of spins in the sample over a range incompatible with the great majority of NMR experiments. While the deleterious consequences of this for spectroscopic resolution are readily appreciated, the consequences for imaging and for sensitivity in general are also severe. This spread of Larmor frequencies over a given sample volume becomes larger as the sensor magnet is made smaller. In Chapter 2, we examine the sensitivity of force-detection in the presence of thermal fluctuations in

the average force on the sensor magnet (Brownian-motion noise), and we find that in order to be near the optimal sensitivity, the sensor magnet, which must be placed as close as possible to the sample, must also be roughly the same size as the sample volume. In this case, the spread of nuclear Larmor frequencies can be of order 30 MHz for sensor magnets composed of the best ferromagnetic materials.

In force-detection methods that couple spin-dependent forces exerted by longitudinal magnetization to oscillatory motion, an rf field near the Larmor frequency is used to invert the sample's magnetization. The spectral range over which spins can be inverted with practical rf fields in nuclear resonance is of order $\sim$100 kHz. As shown in Figure 1.4, in the absence of the annular and other magnets, the field gradient $G_{zz} = \partial B_z / \partial z$ of the sensor magnet and the effective rf field B_1 define a "sensitive slice" through the sample, whose thickness is of order B_1/G_{zz}, outside of which the rf field is ineffective in inverting the spins. These spins therefore do not contribute to the signal energy. In combination with means to scan this surface through the sample volume, this provides an imaging capability[15-17], in which data from separate pixels is collected during separate shots of the experiment, and this approach is called magnetic resonance force microscopy (MRFM). However, this capability is bought at the price of reduced signal energy per shot, in contrast to modern NMR imaging

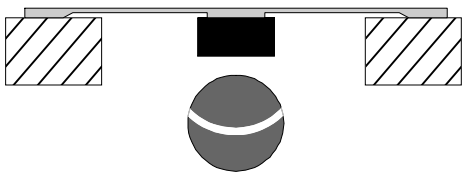

Figure 1.4. Sensitive slice in the sample volume. In the absence of the other parts of the magnet assembly of Figure 1.3, the sensor magnet can spread the Larmor frequencies of spins in the sample over many megahertz. Only those spins within the bandwidth of the applied rf field are inverted during detection.

protocols with higher throughput (*e.g.*, Fourier zeugmatography and back projection)[18], in which signal is acquired during each shot from many pixels, often the whole imaged volume, with the spatial information encoded in the frequency domain by way of field gradients that do not move the magnetization out of the observable spectral range.

The boundaries of the sensitive surface in gradient-based methods of force-detected magnetic resonance[15] are not sharply defined, but instead, the distribution of Rabi frequencies falls off gradually near the edges of the slice[†]. This renders such methods incompatible with modern multiple-pulse sequences that depend upon both a spatially homogeneous Rabi frequency and a spread of Larmor frequencies less than this Rabi frequency to achieve precise, coherent control of the observed spin population through numerous rf pulses.

The problems of reduced spectroscopic resolution, sensitivity, and coherent control will be more severe in NMR of liquids or of molecules weakly bound to a surface, where diffusion out of a sensitive region will occur on a timescale that may be short compared to the time during which either spectral information is to be encoded or during which detection is to take place. In order to suppress the effects of such diffusion, gradient-based methods must be used at lower temperatures or be subject to reduced sensitivity as a result of designs that use larger-than-optimal sensor magnets. This may seriously limit the possibilities for application of such

---

[†] The Rabi frequency characterizes the rate at which the rf field reorients the angle the local magnetization makes with the static field.

methods in chemistry and, especially, biology. The BOOMERANG method minimizes all of these difficulties.

1.3 Outline

In Chapter 2, we quantitatively address the detection of magnetic resonance signals in the presence of thermal noise for the cases of force detection and inductive detection. While this subject has been taken up by several other authors[1,19,20], the indirect, "reciprocity" arguments used by these authors are bypassed herein in favor of a more direct approach that lends itself well to analyses of scaling relations and geometrical optimizations, which are partially obscured by reciprocity arguments. The principal conclusion of Chapter 2 is that in the range of microns to millimeters the signal-to-noise ratio of BOOMERANG force-detected NMR scales with the square-root of the size r of the sample-plus-optimized-detector, while that of traditional inductively detected NMR scales at best as r^2, indicating a sample size (in the $\sim$0.1-1 mm range, depending on the field strength and the magnetogyric ratio of the target spins) below which BOOMERANG detection is preferred.

Chapter 3 introduces the apparatus used in the experiments described in this thesis. The prototype apparatus obtains a variety of NMR data on liquid and solid samples contained within a $\sim$3 mm diameter sample region. The observed signals and noise confirm design principles and the theory of force-detected NMR. Chapter 3 details the magnet assembly and the quantitative assessment of field parameters, the sensor oscillator, the fiber-optic interferometer used to monitor the oscillator's

position, the signal acquisition and conditioning system, rf synthesis and amplification, the NMR coil and sample-holder assembly, and cyclic inversion of the sample's magnetization. Also included is a detailed assessment of system noise sources.

The measurement of various kinds of spectroscopic data with the BOOMERANG prototype forms the subject of Chapter 4. The general notion of time sequencing, in which spectroscopic data are encoded pointwise during a time period separate from the signal-detection period, is used to measure several different kinds of spectroscopic observables. The combination of optimal sensitivity with high resolution has allowed measurement of FT-NMR spectra, longitudinal relaxation times, nutation, spin-echoes with sub-hertz line widths, and heteronuclear *J* spectroscopy in model compounds containing protons and fluorine-19.

Chapter 5 concerns issues that arise in scaling down BOOMERANG NMR to the small numbers of spins in the sample volume possible at the micron size scale and below. The principal subject of this chapter is *spin noise*, which is the uncertainty in measured spectroscopic parameters arising from quantum-thermodynamic fluctuations in the sample's magnetization. These fluctuations, if not accounted for, are an increasingly important source of noise, whatever the method of detection, in the size regime where such fluctuations exceed the mean polarization. The solution suggested herein is measurement of time-correlations of magnetization[21-23]. The correlation signal contains the same information as does the ordinary NMR spectrum, but with roughly unit signal-to-noise ratio per root shot of the experiment, independent of the sample's polarization. Also addressed are

geometrical considerations in application of BOOMERANG to surface-bound or to nanoscopic samples, where, in the latter, the higher mechanical frequencies associated with optimized nanoscopic oscillators suggest coupling torsional oscillators to precessing or spin-locked transverse magnetization at radio frequencies.

References

1 A. Abragam, *Principles of Nuclear Magnetism* (Clarendon Press, Oxford, 1961).

2 J. Wrachtrup, A. Gruber, L. Fleury, and C. von Borczyskowski, *Chem. Phys. Lett.* **267,** 179 (1997).

3 H. Arnolds, D. Fick, H. Unterhalt, A. Voss, and H. J. Jansch, *Sol. St. Nucl. Magn. Reson.* **11,** 87 (1998).

4 R. Tycko and J. A. Reimer, *J. Phys. Chem.* **100,** 13240 (1996).

5 W. G. Jenks, S. S. H. Sadeghi, and J. P. Wikswo, *J. Phys. D Appl. Phys.* **30,** 293 (1997).

6 J. Clarke, *Curr. Opinion Sol. St. & Matl. Sci.* **2,** 3 (1997).

7 C. Connor, *Adv. Magn. Reson.* **15,** 201 (1990).

8 Y. S. Greenberg, *Rev. Mod. Phys.* **70,** 175 (1998).

9 L. G. Gouy, *Compt. Rend.* **109,** 935 (1889).

10 L. N. Mulay, in *Physical Methods of Chemistry*, Vol. I part 4, 4th ed., edited by A. Weissberger and B. W. Rossiter (Wiley-Interscience, New York, 1972), Chapter 7.

11 Y. L. Yousef, R. K. Gigris, and H. Mikhail, *J. Chem. Phys.* **23,** 959 (1955).

12 I. I. Rabi, J. R. Zacharias, S. Millman, and P. Kusch, *Phys. Rev.* **53,** 318 (1938).

13 G. M. Leskowitz, L. A. Madsen, and D. P. Weitekamp, *Sol. St. Nucl. Magn. Reson.* **11,** 73 (1998).

14 D. P. Weitekamp and G. M. Leskowitz, U. S. Patent No. 6,100,687 (California Institute of Technology, USA, 2000).

15 J. A. Sidles, J. L. Garbini, K. J. Bruland, D. Rugar, O. Züger, S. Hoen, and C. S. Yannoni, *Rev. Mod. Phys.* **67,** 249 (1995).

16 O. Züger and D. Rugar, *Appl. Phys. Lett.* **63,** 2496 (1993).

17 O. Züger and D. Rugar, *J. Appl. Phys.* **75,** 6211 (1994).

18 P. Mansfield and P. G. Morris, in *Adv. Magn. Reson.*, Supplement 2 (Academic Press, New York, 1982).

19 D. I. Hoult and R. E. Richards, *J. Magn. Reson.* **24,** 71 (1976).

20 J. A. Sidles and D. Rugar, *Phys. Rev. Lett.* **70,** 3506 (1993).

21 P. J. Carson, L. A. Madsen, G. M. Leskowitz, and D. P. Weitekamp, *Bull. Am. Phys. Soc.* **44,** 541 (1999).

22 P. J. Carson, L. A. Madsen, G. M. Leskowitz, and D. P. Weitekamp, U. S. Patent No. 6,081,119 (California Institute of Technology, USA, 2000).

23 P. J. Carson, L. A. Madsen, G. M. Leskowitz, and D. P. Weitekamp, U. S. Patent No. 6,087,872 (California Institute of Technology, USA, 2000).